Cement & Concrete Composites 34 (2012) 1149–1158

Contents lists available at SciVerse ScienceDirect

Cement & Concrete Composites

journal homepage: www.elsevier.com/locate/cemconcomp

Failure processes of modeled recycled aggregate concrete under uniaxial compression

Wengui Li [a,b], Jianzhuang Xiao [a,*], Zhihui Sun [c], Surendra P. Shah [b]

[a] Department of Building Engineering, Tongji University, Shanghai 200092, PR China
[b] Center for Advanced Cement-Based Materials, Northwestern University, Evanston, IL 60208, USA
[c] Department of Civil & Environmental Engineering, University of Louisville, Louisville, KY 40292, USA

ARTICLE INFO

Article history:
Received 8 July 2011
Received in revised form 28 June 2012
Accepted 29 June 2012
Available online 15 July 2012

Keywords:
Modeled recycled aggregate concrete
Failure process
Uniaxial compression
Digital image correlation (DIC)
Crack propagation

ABSTRACT

In order to investigate the failure processes of Recycled Aggregate Concrete (RAC), cracking behavior of modeled RAC specimens under compressive loading was investigated using Digital Image Correlation (DIC). Strain and displacement contour maps were produced to analyze the cracks' initiation and propagation during loading. The testing results indicate that the discrepancy between the elastic moduli of coarse aggregates and mortar matrix significantly influences the mechanical properties and crack patterns of the modeled materials. It is found that the failure process is related to the relative strength of coarse aggregate and mortar matrix. For modeled RAC, the first bond cracks appear around both the old and new interfacial transition zones (ITZ), and then propagate into the old and new mortar matrix by connecting each other. The observation implies that the initiations and propagations of microcracks are different between RAC and Natural Aggregate Concrete (NAC). The findings in this investigation are useful to improve the mechanical properties of RAC by optimizing the mix proportion.

1. Introduction

The coarse aggregates in concrete are often modeled as inclusions in a matrix of mortar [1]. The mismatch between the elastic moduli of the coarse aggregates and the mortar matrix causes stress concentration when concrete is loaded. The modes of crack opening especially around the coarse aggregates and the angles at which mortar cracks originate and propagate are essential to understanding the failure process of cement-based materials. In the past, many attempts have been made to explain the complex behaviors of concrete with the help of various models [2,3]. Among different modeling approaches, using modeled concrete was found to be effective to study the cracking process in concrete. Modeled concrete is a concrete model, which uses aggregates in particular shape and sizes to assist studying the complex behavior of concrete under loading, e.g. crack initiation and propagation. Model concrete specimens that contain different number of embedded limestone aggregates (1, 5, and 13 aggregates) were examined by Choi and Shah [4] to establish the relationship between the fundamental fracture processes and the aggregate spacing. Corr et al. [5] used single aggregate and two-aggregate modeled concrete to study the bond property of interfacial transition zones between aggregates and cement paste.

The depletion of supply of qualified aggregates together with environmental, economic, and energy considerations encourage the usage of Recycled Coarse Aggregate (RCA) in new concrete constructions [6–9] to make Recycled Aggregate Concrete (RAC). It has been demonstrated that the earthquake debris can be recycled as aggregates which was considered as part of the strategy for reconstruction in earthquake-hit areas [10,11]. The majority of RCA applications for pavements and airfields have been primarily carried out all over the world [12,13]. It is widely accepted [14,15] that the Interfacial Transition Zone (ITZ), both between the original aggregate and adhered mortar, and between the recycled aggregates and new mortar, complicate the analysis of cracking and failure of RAC.

The presented work mainly focuses on evaluating the failure processes of modeled RAC under uniaxial compression. Three types of coarse aggregates were used in this study: natural granite (in the form of cylindrical cores taken from stone) and two types of recycled aggregates also in cylindrical shape. In addition to the three forms of modeled concrete, cement mortar specimens (without coarse aggregates) were also studied to analyze the influence of material uniformity on fracture. A two-dimensional Digital Image Correlation (DIC) technique was applied to obtain the whole-field deformation characteristics and maps of crack's propagations on the specimen surfaces in real time [5,16,17]. This investigation will provide insights into the failure processes of both recycled aggregate concrete and Natural Aggregate Concrete (NAC).

* Corresponding author. Tel.: +86 21 65982787; fax: +86 21 65986345.
E-mail address: jzx@tongji.edu.cn (J. Xiao).

0958-9465/$ - see front matter © 2012 Elsevier Ltd. All rights reserved.
http://dx.doi.org/10.1016/j.cemconcomp.2012.06.017

(a) Natrual coarse aggregate (NCA) (b) Recycled coarse aggregate (RCA) (c) Cored coarse aggregate (CCA)

Fig. 1. Types of coarse aggregate.

2. Experimental program

2.1. Specimen preparation

This study considers concrete as a composite material where the inclusions (coarse aggregates) are embedded in a continuous matrix (cement mortar), both phases interact through the ITZ. The series of modeled concretes were composed of a mortar matrix, in which nine circular discs of coarse aggregates were embedded in a square array [3]. As for the nature of the heterogeneity of a modeled concrete composite, the coarse aggregate can be considered as an inclusion within a continuous mortar matrix.

The present different basic modeled specimens were prepared to obtain as nearly as possible a state of plane stress. Different modeled specimens with three types of cylindrical coarse aggregates were used in this study: natural coarse aggregate (NCA), recycled coarse aggregates (RCA) and cored coarse aggregate (CCA) as shown in Fig. 1. The NCA with a diameter of 38 mm was obtained by drilling granite stones. The RCA with a diameter of 38 mm was obtained by drilling a thin plate with old mortar (180 days age) which was adhered to NCA. The CCA with a diameter of 38 mm was cored out from old conventional concrete plate. All of the three kinds of cylindrical coarse aggregates with the same height (30 mm) were used for different modeled concrete, respectively. The mortar compositions used for all the three modeled concrete were kept the same.

Table 1 lists the related properties of the NCA and CCA including sizes, compressive strength and elastic moduli. From Table 1, a significant difference in mechanical properties between NCA and CCA was found from laboratory testing results. The compressive strength of NCA is about five times higher than that of CCA and the NCA's elastic moduli are also approximately twice as much as those of CCA. The elastic moduli of NCA and CCA were measured according to GB/T50081-2002 [18]. For the RCA, the thickness of the adhering old mortar around the cylindrical granite is approximately 5 mm. The mix proportion and mechanical properties of old hardened mortar that used to prepare RCA as well as new hardened mortar used for all the three modeled concrete are presented in Tables 2 and 3, respectively. Both mortars have a water-to-cement ratio of 0.45. The compressive strengths of new and old cement mortar were the average of three testing results on cubes of 70.7 mm × 70.7 mm × 70.7 mm according to JGJ/T70-2009 [19]. From Table 3, it can be seen that both the strength and the moduli of new mortar were similar with those of the old mortar. The old mortar was used for prepared RCA, while the new mortar was used for casting all the specimens.

The three different modeled cement-based materials with a same dimension of 150 mm × 150 mm × 30 mm contained different cylindrical coarse aggregates and cement mortar are shown in Fig. 2, including modeled natural aggregate concrete (MNAC), modeled recycled aggregate concrete (MRAC), modeled cored aggregate concrete (MCAC) and cement mortar (CM). The MNAC was used to simulate conventional concrete, and the MRAC and MCAC were used to simulate recycled aggregate concrete, whereas the CM was used for comparisons.

Table 1
Properties of coarse aggregates.

Type	Diameter (mm)	Height (mm)	Compressive strength (MPa)	Elastic modulus (GPa)
NCA	28	30	247.8	83
CCA	38	30	51.4	41

The listed results were obtained based on the average of three specimens.

Table 2
Mixture proportion of new and old mortar.

Type	Unite mass (kg/m^3)			Water to cement ratio
	Water	Cement	Sand	
Old hardened mortar	160	320	565	0.45
New hardened mortar	190	420	640	0.45

Table 3
Mechanical properties of old and new cement mortar.

Type	Compressive strength (MPa)	Elastic modulus (GPa)
Old hardened mortar	75.3	33.7
New hardened mortar	74.4	33.3

The listed results were obtained based on the average of three specimens.

When casting the modeled concrete, the aggregates were first placed vertically in steel molds, and the new mortar was then filled in around them with the aid of a vibration table. After being kept in the laboratory for 24 h, the mold was removed and the specimens were kept underwater for 90 days until testing. For each kind of molded cement-based materials, there are three duplicates prepared in this study.

2.2. Testing procedure

The current experimental system consists of three parts: a digitally controlled servo-hydraulic loading system, a computer vision DIC system and DIC analysis software, as displayed in Fig. 3. The compressive loading was performed in an INSTRON-5592 SATEC servo-hydraulic testing machine with a capacity of 6000 kN. The loading was applied with a displacement control and the loading rate was controlled at 0.02 mm/min to obtain the post-peak behavior of modeled specimens. Two Teflon sheets of 0.2 mm thick were

(a) Modeled natural aggregate concrete (MNAC)

(b) Modeled recycled aggregate concrete (MRAC)

(c) Modeled cored aggregate concrete (MCAC)

(d) Cement mortar (CM)

Fig. 2. Types of prepared modeled cement-based materials.

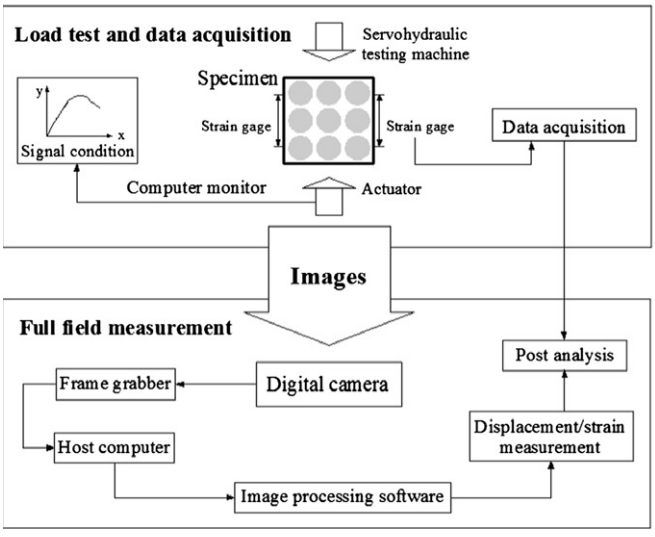

(a) Schematic of DIC measurement

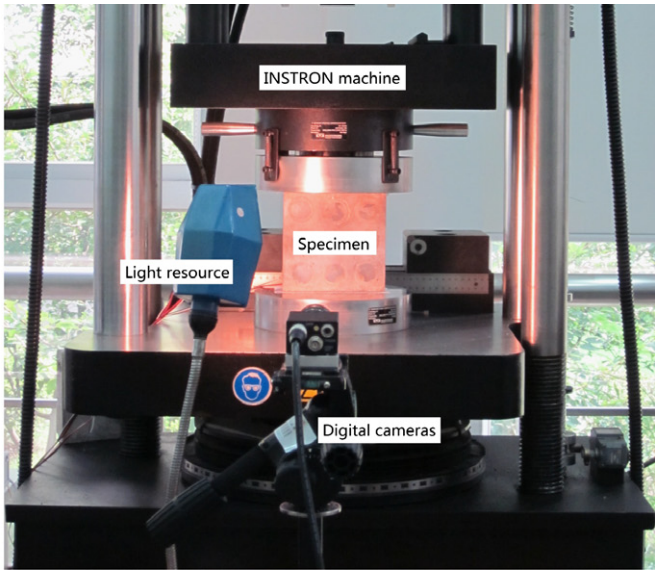

(b) Setup at the testing site

Fig. 3. Setup for loading test and DIC measurement.

inserted between the specimen and the machine loading plates to reduce the frictional shear constraints [20,21]. Within the pre-peak loading range, the vertical strains of the specimen were measured by the strain gauges [22–24]. The vertical deformation of the specimen between loading platens was measured by self-mounted displacement transducer of the testing machine. Up to the peak load,

the surface strain measurement was regarded as the global strain measurement. After the peak load, the deformation of interlayer and loading system were left out of consideration in the global deformation measured by the self-mounted crosshead displacement extensometers. So the global vertical strain was obtained by strain gauges in the pre-peak range and self-mounted transducer within the post-peak range [25].

The whole front surface of each specimen was captured with a camera of the digital image correlation system during testing. The image size was 160 mm × 160 mm, thus covering the complete specimen size of 150 mm × 150 mm. The imaging system based on DIC was composed of a monochrome 8.5 mm CCD camera with a resolution of 2560 × 2160 pixels (256 gray levels) and a PCVISION plus image grabber [26]. The measurement resolution of the current DIC system was approximately 74 μm. The image analysis software (Optical Fringe Pattern Analysis) was then used to calculate the displacements and strain distribution over the specimen surface. As the modeled concretes under uniaxial compression can be considered as a state of plane stress, the 2D-digital image correlation was capable of examining the two-dimensional cracking propagation on the specimen surface [27].

3. Experimental results

3.1. Stress–strain curves

The difference between the elastic moduli of aggregates and that of hardened mortar influences the bond stresses between the two materials and the shape of the stress–strain curve [28,29]. The mean stress–strain curves for each modeled specimens and cement mortar are compared and shown in Fig. 4. The letters from *a* to *e* in Fig. 4 denote five loading stages, i.e., 15%, 45%, 75% and 100% of peak load in the pre-peak range, and 85% of peak load in the post-peak range. Moreover, the numbers from 1 to 4 indicate each corresponding materials as listed in Fig. 4, i.e., 1 indicates MNAC and 4 indicates CM. It can been seen clearly that the stress–strain curves of the modeled specimens do not match each other, which indicate a strong influence of coarse aggregates that used. Table 4 shows the elastic moduli, peak stress and peak strain for the three modeled concrete together with CM. It is found that the peak stress of MNAC was 17% and 24% higher than that of MRAC and MCAC, respectively. However, the peak strain of MNAC was lower than that of MRAC and MCAC. The reduction in the compressive strength of MRAC compared to MNAC

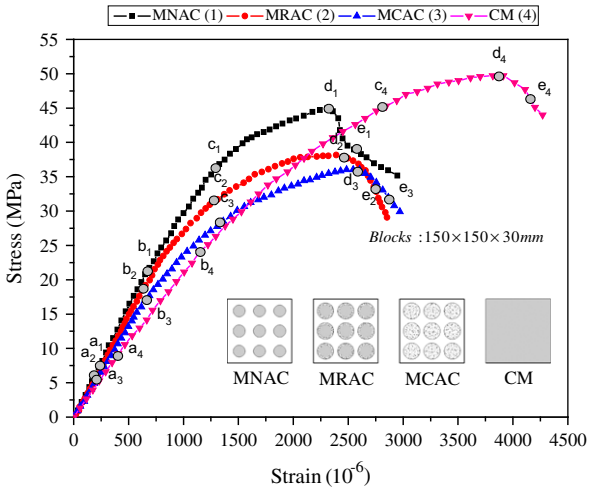

Fig. 4. Loading stages numbered on stress–strain curves of different modeled specimens.

Table 4
Mechanical characteristics of four different modeled cement-based materials.

Type	Elastic modulus (GPa)	Peak stress (MPa)	Peak strain (με)
MNAC	30.26	44.53	2307
MRAC	28.62	38.14	2378
MCAC	25.98	36.04	2486
CM	21.78	49.70	3913

Each type of modeled cement-based materials has three specimens.

was due to the existence of adhered mortar and the old interfacial transition zone which were considered as a weak part in recycled aggregate concrete [30,31]. The elastic moduli of coarse aggregate have a significant influence on the elastic moduli of concrete. Because the elastic modulus of CCA was 50% lower than that of NCA, the compressive strength and elastic moduli of MCAC are decreased 14% and 5% compared to those of MNAC, respectively. In CM, the composite of mortar matrix was relative uniform, resulting in a highest peak stress and strain among the four materials.

The axial deformation of modeled specimens was recorded using DIC method. The strain of the front surface of the modeled specimens was measured with the DIC system by stacking images obtained at different stages of loading. To calculate the axial strain, three couples of points were chosen in the front specimen surface with a height of 100 mm, which were located on the left, middle and right part, respectively. The average axial strains were calculated from the three couples of points. The stress–strain curves measured by strain gages and DIC method show a good agreement as displayed and compared in Fig. 5. The slight difference between strain gages and DIC measurements can be attributed to the accuracy of the DIC and surface conditions of specimen. The relationships between the lateral and axial strains of different modeled concretes obtained by DIC technique is summarized and depicted in Fig. 6. The axial strain at the beginning was introduced due to the vertical deformation of the specimen, while the lateral strain was introduced due to the lateral dilation of the specimen. The CM which did not contain coarse aggregates exhibited the almost uniform deformation before the peak load. On the other hand, the lateral deformations in the MNAC, MRAC and MCAC which stemmed from the growth of microcracks and failure of interfacial bonds showing continuous increase through the whole pre-peak range. Hence, the failure processes in these modeled specimens started from a very early loading stage and developed gradually with the increase of loading. During the pre-peak loading stage, the lateral deformation of MRAC and MNAC were more obvious than that of MNAC. It indicates that there are more microcracks existed in the MRAC and MCAC than MNAC within the pre-peak loading range.

3.2. Failure process

The accuracy of displacement and strain measurements obtained from DIC technique depends on the quality of speckle pattern, surrounding vibrations, lighting, out-of-plane displacements and specimen height used for strain computations, etc. [32]. The displacement contour maps obtained from the DIC system can show detailed crack patterns of modeled concretes. On the other hand, the small strain concentrations distribution can provide information about the microcracks initiation and development [33].

The description of lateral strain and displacement distribution of modeled concretes obtained from DIC method at different stages of loading were shown in Figs. 7–14. The strain contour maps were obtained from DIC measurement system at four loading stages (15%, 45%, 75% and 100% of peak load in pre-peak range, as shown

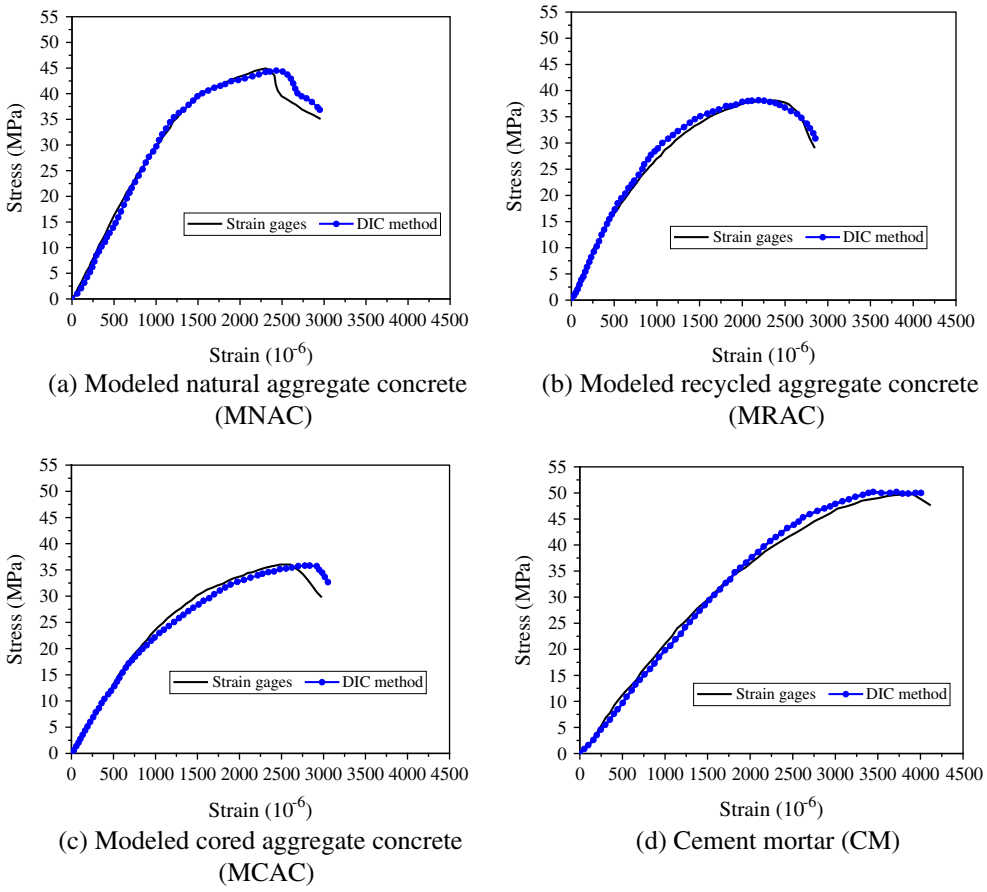

Fig. 5. Relationship between axial displacement from strain gages and DIC method.

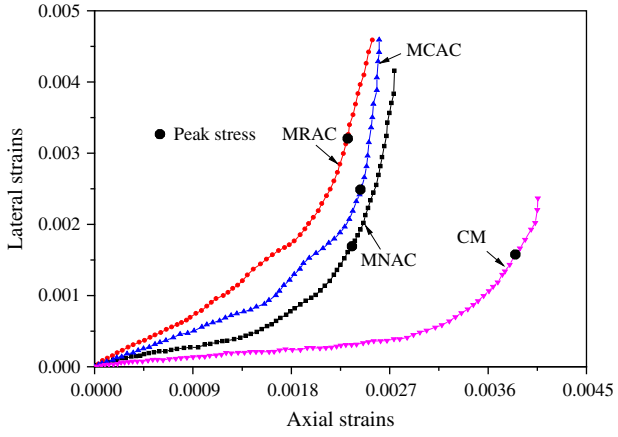

Fig. 6. Comparison between axial strain and lateral strain.

in Fig. 4). The displacement contour maps were obtained at other four loading stages (50%, 75%, 100% of peak load in the pre-peak range, and 85% of peak load in the post-peak range, as shown in Fig. 4).

3.2.1. Modeled natural aggregate concrete

Fig. 7 presents the lateral strain distribution contour maps of MNAC at different loading stages. It is found that a substantial amount of observable microcracks was examined at about 75% of the peak load in the interfacial transition zones of MNAC. Microcracks formed around the NCA while some cracks formed extensively in the mortar matrix. With the increase of loading, microcracks and mortar matrix cracks started to connect with each other, forming the global fracture in the post-peak loading stage.

Fig. 8 shows the lateral displacement distribution contour maps of MNAC at four different loading stages. In the final crack pattern, most cracks lined up vertically with the loading direction. In the mortar region of MNAC, vertical splitting crack patterns were obviously detected on the specimen surface.

3.2.2. Modeled recycled aggregate concrete

Fig. 9 shows typical lateral strain distribution contour maps of MRAC at four loading stages. According to the final failure of MRAC, it appeared that the observable microcracks appeared at both the old and new ITZ regions. A substantial amount of microcracks exist around both the new and old ITZs within the pre-peak loading stage for MRAC. With the loading increase, the microcracks tended to evolve into major global cracks. Each group of cracks started connecting with others, forming a global failure band around the peak load. For MRAC, most of the cracks developed around aggregates, and then traversed the old mortar and propagates into new mortar matrix.

Fig. 10 shows typical lateral displacement distribution contour maps of MRAC at four different loading stages. The bond cracks around the new and old ITZs developed across old cement mortar, and propagated into new cement mortar vertically with the increasing load.

3.2.3. Modeled cored aggregate concrete

Fig. 11 presents typical lateral strain distribution contour maps of MCAC at four different loading stages. It was observed that

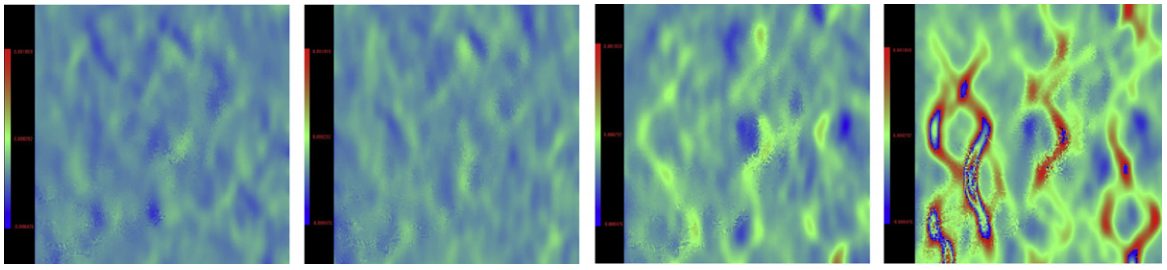

(a) a_1 (15% of peak load) (b) b_1 (45% of peak load) (c) c_1 (75% of peak load) (d) d_1 (100% of peak load)

Fig. 7. Contour maps of lateral strain field for MNAC.

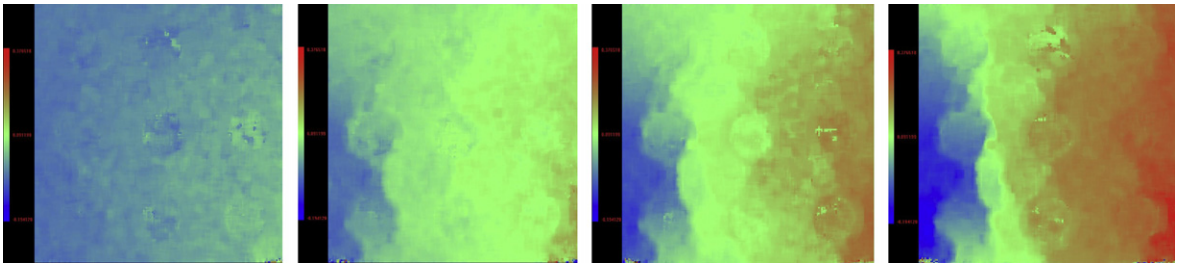

(a) b_1 (45% of peak load) (b) c_1 (75% of peak load) (c) d_1 (100% of peak load) (d) e_1 (85% of peak load)

Fig. 8. Contour maps of lateral displacement field for MNAC.

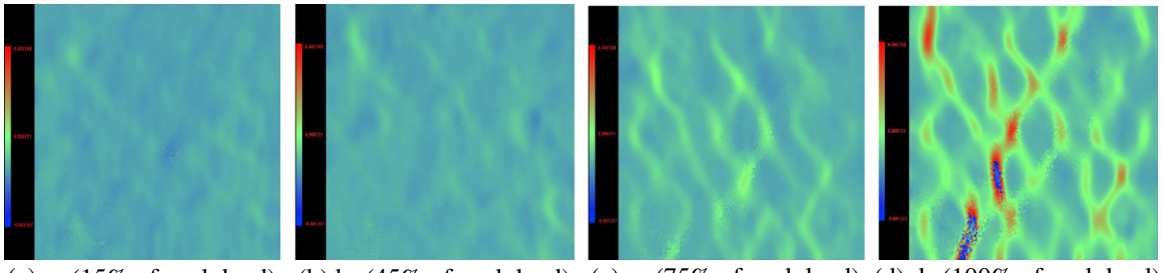

(a) a_2 (15% of peak load) (b) b_2 (45% of peak load) (c) c_2 (75% of peak load) (d) d_2 (100% of peak load)

Fig. 9. Contour maps of lateral strain field for MRAC.

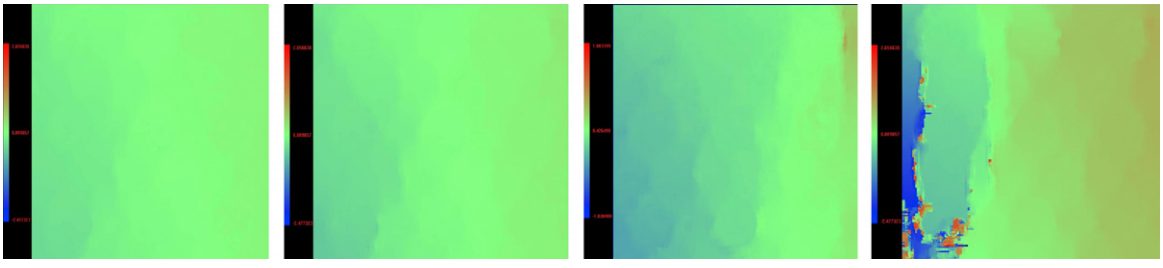

(a) b_2 (45% of peak load) (b) c_2 (75% of peak load) (c) d_2 (100% of peak load) (d) e_2 (85% of peak load)

Fig. 10. Contour maps of lateral displacement field for MRAC.

microcracks firstly appeared both in the ITZs and mortar regions. With the load increased, vertical cracks originated predominantly from the interfacial cracks and propagated vertically in the mortar matrix. Some of them near the top and bottom part of the specimen traverse through cored aggregates. It indicates that the strength of MCAC can be influenced by the strength of the CCA.

Fig. 12 shows typical lateral displacement distribution contour maps of MCAC at different loading stages. Both vertical crack bands combined with shear cracks bands were observed for MCAC. The cracks in MCAC showed more distributed angles, but 80% of those cracks angles were less than 30°.

3.2.4. Cement mortar

Fig. 13 presents the lateral strain distribution contour maps of CM at four different loading stages. It was examined that the CM revealed almost uniform response up to the peak load. The lateral

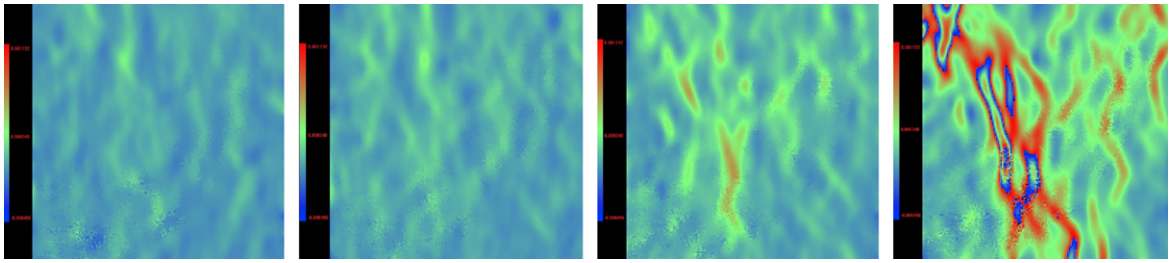

(a) a_3 (15% of peak load) (b) b_3 (45% of peak load) (c) c_3 (75% of peak load) (d) d_3 (100% of peak load)

Fig. 11. Contour maps of lateral strain field for MCAC.

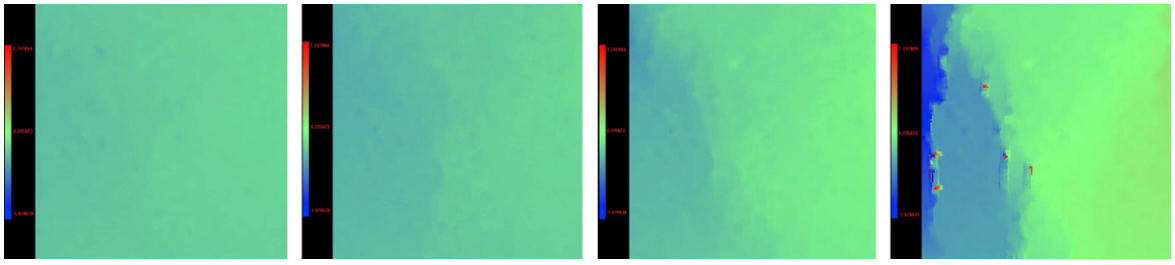

(a) b_3 (45% of peak load) (b) c_3 (75% of peak load) (c) d_3 (100% of peak load) (d) e_3 (85% of peak load)

Fig. 12. Contour maps of lateral displacement field for MCAC.

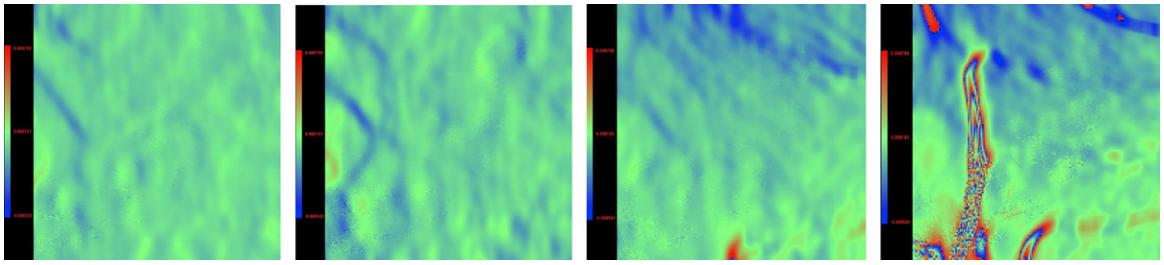

(a) a_4 (15% of peak load) (b) b_4 (45% of peak load) (c) c_4 (75% of peak load) (d) d_4 (100% of peak load)

Fig. 13. Contour maps of lateral strain field for CM.

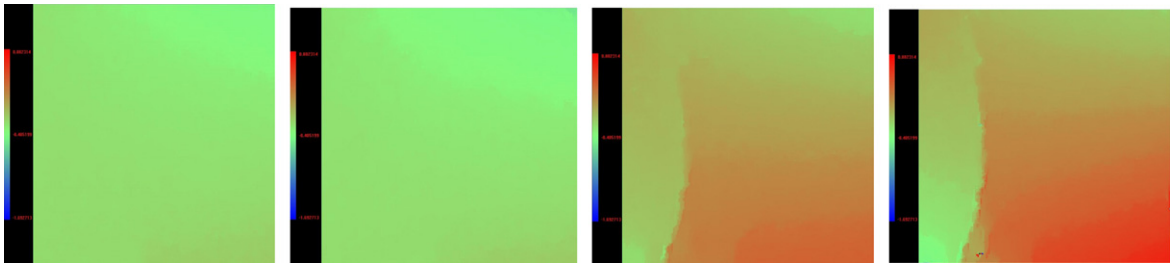

(a) b_4 (45% of peak load) (b) c_4 (75% of peak load) (c) d_4 (100% of peak load) (d) e_4 (85% of peak load)

Fig. 14. Contour maps of lateral displacement field for CM.

strain was uniformly distributed in CM up to 75% of peak load. With the increase of loading, the cracks did not uniformly develop on the specimen surface, which locally concentrated and grew vertically.

Fig. 14 shows typical lateral displacement distribution contour maps of CM at four different loading stages. It was observed that a single crack initiated before the peak load and propagated in the loading direction at post-peak range. The main crack propagated almost over the whole height of the specimen.

4. Analysis and discussions

4.1. Mechanical properties

The research proves again that the discrepancy between the elastic moduli of coarse aggregate and mortar matrix has a significant contribution to the cracking modes of the specimen when subjected to loading. In this study, the elastic modulus of NCA was much higher than that of mortar matrix in MNAC. Therefore,

the elastic mismatch of aggregate and mortar in MNAC caused highly non-uniform deformation at the ITZs in MNAC. In both MRAC and MCAC, the elastic moduli of coarse aggregates were relatively closer to that of mortar, resulting in less non-uniform deformation at the interfaces. For the CM, the deformation was much more uniform compared to all the other specimens.

The peak strain from the compression showed a minimum value in the MNAC. Among MRAC, MCAC and CM, relatively higher values of peak strain was obtained in CM due to the elastic consistency of the constituents. It indicates that with the same mix proportion, the mechanical properties of recycled aggregate concrete appear relatively lower than those of natural aggregate concrete. However, because the mismatch between the elastic moduli of coarse aggregate and mortar matrix in recycled aggregate concrete (RAC) is less obvious than that in natural aggregate concrete (NAC), the peak strain of RAC is higher than that of NAC.

4.2. Cracking modes

The microcrack developments in the modeled cement-based materials are illustrated in Fig. 15 and 16. As shown in Fig. 16, the primary failure mode in CM was found to be mode I. For the MNAC and MRAC and MCAC, both mode I and mode II were observed in the mortar matrix, and mixed modes were also found around the ITZs. In modeled concrete, the cracks in the mortar matrix can be characterized by either the mode I or the mode II, while the cracks around the ITZs could be characterized by the mixed mode.

The main crack in CM angled less than 10° from the loading direction. The cracks in MNAC, MRAC and MCAC show more distributed angles, but most cracks angled less than 30° (except around the coarse aggregate). The crack propagation angles strongly depended on the materials composition or the types of coarse aggregate. In CM, a single crack initiated at the peak load and propagated in the loading direction. The cracks in MNAC, MRAC and MCAC, which were observed prior to the peak load, were much more complicated. Both vertical cracks and inclined cracks were observed. For MNAC, the microcracks were found at the ITZ and grew vertically in mortar matrix region. In MRAC microcracks were observed around both the new and old ITZs, and propagated across the old mortar matrix and new mortar matrix connecting with each other. For MCAC, cracks were likely to develop around the ITZs, but sometimes propagated through the cored coarse aggregates. The experimental observations indicate that microcracks initiated around both old and new ITZ in MRAC, while for MNAC microcracks just appeared around the ITZ between NCA and cement mortar. It can be concluded that there are more weak regions existing in RAC than those in NAC.

4.3. Failure modes

The detailed information on the failure modes of the four modeled specimens was shown in Fig. 17, in which the widths of cracks were measured by image analysis (Image Pro software). The crack marked with ***A*** has a tendency to propagate parallel to the loading direction in the mortar matrix. Most the type ***A*** cracks go around the coarse aggregate, although sometimes they pass through aggregate. Crack marked with ***B*** shows opening cracks in lateral direction, which implies that only mode I cracking exists. On the other hand, the crack marked with ***C*** reveals both lateral and ver-

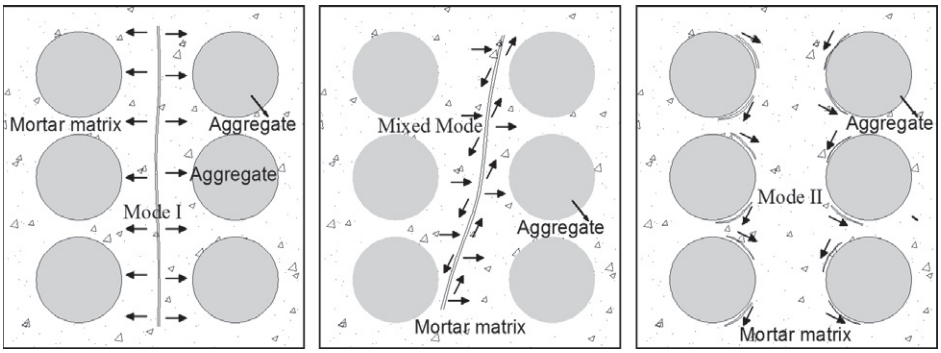

Fig. 15. Schematic diagram of different cracking modes.

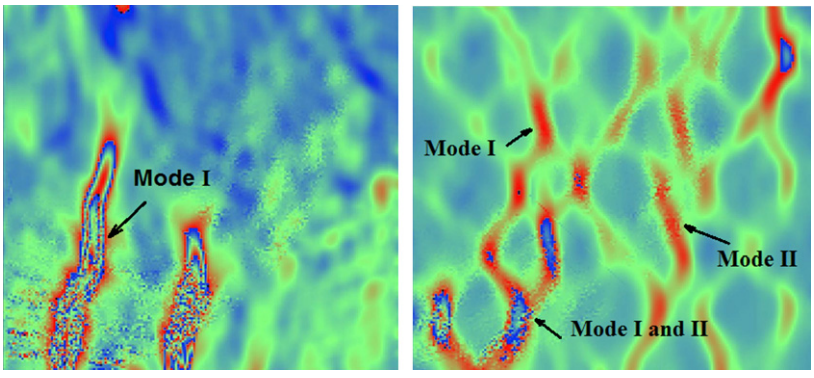

Fig. 16. Cracking modes in modeled cement-based materials.

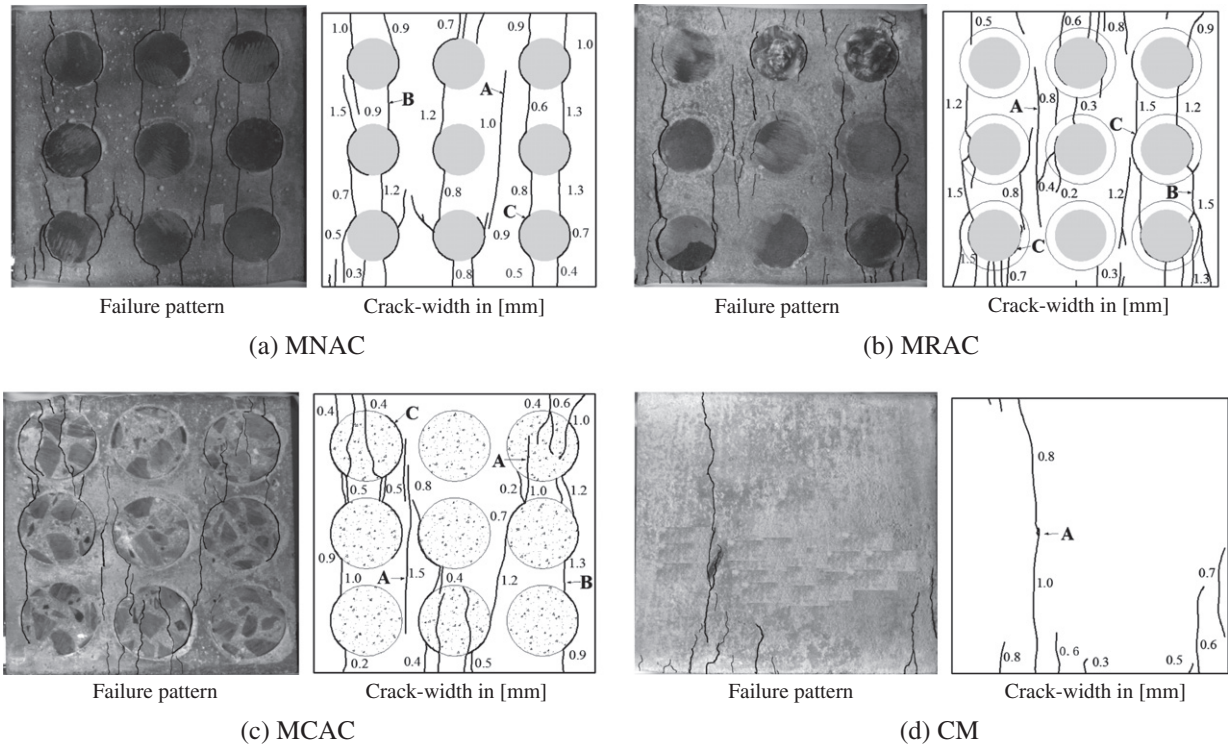

Fig. 17. Failure modes of modeled cement-based materials.

tical openings, indicating a mixed mode cracking. For MNAC, the type ***C*** cracks appeared around the ITZs regions, and type ***A*** and type ***B*** cracks were found in the mortar matrix. Most Type ***C*** cracks were observed around both new and old ITZs region. In MRAC, the cracks were observed at both old and new ITZs. Globally, primarily vertical cracks for MNAC and MRAC were similar to each other. However, the crack propagation around coarse aggregate was somewhat different because MRAC has two kinds of ITZs compared to MNAC. In MCAC, type ***C*** cracks occurred and developed at the interfaces between CCA and mortar matrix. Most type ***A*** and ***B*** cracks propagated around the ITZ, but some of them passed through CCA. In the CM, type ***A*** cracks were primarily examined around the peak load along the loading direction. It was shown that the crack initiation and propagation in recycled aggregate concrete is different from that of natural aggregate concrete, but the global failure patterns for them are similar.

The MRAC can be used to simulate the failure processes of real RAC. As the test results of MRAC shown, bond cracks first appeared around the weak ITZs, and then propagated into the mortar regions. Moreover, the microcracks' locations, sizes, and shapes in the ITZs were influenced by the relative strength of the old mortar matrix and new mortar matrix. In this study, the strength of the old mortar was close to that of new mortar. As a result, the observable cracks appeared at both the old ITZ and new ITZ. Also, the cracks development of MCAC depends on the relative strength of CAC and new mortar. When the strength of CAC is weaker than that of new mortar, the cracks probably go through the CAC in MCAC. It implies that the failure mode of RAC is significantly influenced by the relative strength of recycled coarse aggregate and new mortar. So, it can be found that there are some similarities in the failure processes between MRAC and real RAC.

5. Conclusion

Modeled cement-based materials were designed to investigate the failure processes of natural aggregate concrete and recycled aggregate concrete under uniaxial compression. The related conclusions are summarized as follows:

(1) Compared to MNAC, MRAC and MCAC presented lower elastic moduli and compressive strength. On the other hand, the peak strain of MRAC and MCAC were relatively higher than that of MNAC probably due to the greater elastic compatibility between coarse aggregates and mortar matrix.
(2) The global cracks basically developed along the loading direction for all the modeled cement-based materials. For MNAC, the first crack appeared around the ITZ, and then propagated into the mortar matrix. In MRAC, the initial cracks occurred around both new and old ITZs, and propagated across the old mortar region connecting with each other. In MCAC, some of the cracks traversed through cored coarse aggregates.
(3) The observations also indicate that the discrete crack model (Mode I) can be used to describe the failure of CM, while the multiple sliding crack models can describe the crack patterns observed in MNAC, MRAC and MCAC. The global failure patterns of MRAC were similar to that of MNAC. Mixed mode behavior was obviously found around the ITZs in both MRAC and MCAC.
(4) Understanding of the differences in the failure processes between MRAC and MNAC can provide insights into the failure mechanism of recycled aggregate concrete. Such understanding can be used to improve the mechanical properties of recycled aggregate concrete through optimization of the mixture proportions.

Acknowledgments

The authors gratefully acknowledge support from the National Natural Science Foundation of China (51178340), the Kwang-Hua Foundation, and the Shanghai Science and Technology Committee

(10231202000). The authors also gratefully thank Prof. David J. Corr in Northwestern University as well as Shanghai Institute of Ceramics and Shanghai University for the test technical supports.

References

[1] Bremner TW, Holm TA. Elastic compatibility and the behavior of concrete. ACI J Proc 1986;83(2):244–50.
[2] Shah SP, Winter G. Inelastic behavior and fracture of concrete. ACI Spec Pub 1968;20:5–28.
[3] Buyukozturk O, Nilson AH, Slate FO. Stress–strain response and fracture of concrete in biaxial loading. ACI J Proc 1971;68:590–9.
[4] Choi S, Shah SP. Propagation of microcracks in concrete studied with subregion scanning computer vision (SSCV). ACI Mater J 1999;96(2):255–60.
[5] Corr D, Accardi M, Graham-Brady L, Shah S. Digital image correlation analysis of interfacial debonding properties and fracture behavior in concrete. Eng Fract Mech 2007;74(1–2):109–21.
[6] Xiao JZ, Li WG, Fan YH, Huang X. An overview of study on recycled aggregate concrete in China (1996–2011). Constr Build Mater 2012;31(6):364–83.
[7] ACI Committee 555. ACI 555–01: removal and reuse of hardened concrete. Am Conc Inst; 2001.
[8] Topçu IB, Günçan NF. Using waste concrete as aggregate. Cem Concr Res 1995;25(7):1385–90.
[9] Wu B, Zhao XY, Liu QX. Full-scale axial loading tests of concrete-filled steel tubular columns incorporating demolished concrete lumps. RILEM Proc 2010;73:36–45.
[10] DesRoches RR, Kurtis KE, Gresham JJ. Breaking the reconstruction logjam: Haiti urged to recycle concrete rubble. Am Ceram Soc Bull 2011;90(1):20–6.
[11] Xiao JZ, Xie H, Zhang Ch. Investigation on building waste and reclaim in Wenchuan earthquake disaster area. Resour Conserv Recy 2012;61(4):109–17.
[12] Bekoe PA, Tia M, Bergin MJ. Concrete containing recycled concrete aggregate for use in concrete pavement. J Transport Res Board 2010;21(64):113–21.
[13] Bordelon A, Cervantes V, Roesler JR. Fracture properties of concrete containing recycled concrete aggregates. Mag Concr Res 2009;61(9):665–70.
[14] Du T, Wang WH, Lin HL, Liu ZX, Liu J. Experimental study on interfacial strength of the high performance recycled aggregate concrete. ASCE Conf Proc 2010;10:2821–8.
[15] Nagataki S, Gokce A, Saeki T, Hisada M. Assessment of recycling process induced damage sensitivity of recycled concrete aggregates. Cem Concr Res 2004;34(6):965–71.
[16] Choi S, Shah SP. Fracture mechanism in cement-based materials subjected to compression. J Eng Mech 1998;124(1):94–102.
[17] Caduff D, Van Mier JGM. Analysis of compressive fracture of three different concretes by means of 3D-digital image correlation and vacuum impregnation. Cem Concr Compos 2010;32(4):281–90.
[18] GB/T 50081–2002. National standard of the P.R. China. standard for test method of mechanical properties on ordinary concrete; 2002 [in Chinese].
[19] JGJ/T70-2009. Trade standard of the P.R. China. Standard for test method of performance on building mortar; 2009 [in Chinese].
[20] Van Mier JGM, Shah SP, Arnaud M, Balayssac JP, et al. Strain-softening of concrete in uniaxial compression. Mater Struct 1997;30(4):195–209.
[21] Choi S, Thienel KC, Shah SP. Strain softening of concrete in compression under different end constraints. Mag Concr Res 1996;48(175):103–15.
[22] Van Mier JGM. Multiaxial strain-softening of concrete. Part I: fracture. Mater Struct 1986;19(111):179–90.
[23] Davide Z. Microstructural characterization of the fracture path in cement paste and mortar through surface roughness measurements of the paste portion. PhD thesis. Evanston (IL): Northwestern University; 1997.
[24] Jansen DC, Shah SP, Rossow EC. Stress–strain results of concrete from circumferential strain feedback control testing. ACI Mater J 1995;92(4):419–28.
[25] Wang ZL. Study and application of mesoscopic mechanical model of concrete based on the discrete element method. PhD thesis. Shanghai, China: Tongji University; 2009 [in Chinese].
[26] Zhang DS, Luo M, Arola DD. Displacement/strain measurements using an optical microscope and digital image correlation. Opt Eng 2006;45(3):033605.
[27] Shen B, Paulino GH. Direct extraction of cohesive fracture properties from digital image correlation: hybrid inverse technique. Exp Mech 2011;51(2):143–63.
[28] Tasdemir MA, Tasdemir C, Akyüz S, Jefferson AD, Lydon FD, Barr BIG. Evaluation of strains at peak stresses in concrete: a three-phase composite model approach. Cem Concr Compos 1998;20(4):301–18.
[29] Neville AM. Aggregate bond and moduli of elasticity of concrete. ACI J Proc 1997;94(1):71–4.
[30] Xiao JZ, Li JB, Zhang C. Mechanical properties of recycled aggregate concrete under uniaxial loading. Cem Concr Res 2005;35(6):1187–94.
[31] Du T, Wang WH, Liu ZX, Lin HL, Guo TP. The complete stress–strain curve of recycled aggregate concrete under uniaxial compression loading. J Wuhan Univ Technol (Mater Sci Ed) 2010;25(5):862–5.
[32] Shah SG, Chandra Kishen JM. Fracture properties of concrete–concrete interfaces using digital image correlation. Exp Mech 2011;51(3):303–13.
[33] Van Mier JGM. Framework for a generalized four-stage fracture model of cement-based materials. Eng Fract Mech 2008;75(18):5072–86.